

SUPPLEMENTAL MATERIAL AND METHODS

Animal model. *Pkhd1*^{del4/del4} mice were generated on a mixed C57BL6/129Sv background, which possesses an inactivating deletion in the exon 4 of the *Pkhd1* gene (orthologous of the human PKHD1) and is WT littermates of the same genetic background served as controls. Genotype for each mouse was determined by PCR. After mouse sacrifice, liver tissue was harvested, fixed in formalin and embedded in paraffin (two main lobes). To prevent the risk of concurrent biliary tract infections which theoretically could contribute to the generation of a portal inflammatory infiltrate, in *Pkhd1*^{del4/del4} (n=11) and WT (n=10) mice of 3 months of age bowel decontamination was performed with polymyxin B (to bind endotoxins) (100 mg) and neomycin (220 mg/Kg body weight/day) added to the drinking water for 3 months. Microbiological analysis of liver samples was performed after animal sacrifice.

Assessment of portal fibrosis by Sirius Red staining. Sections stained by Sirius Red were analyzed with a Nikon Eclipse TE2000U microscope at polarized light (Nikon, Florence, Italy) by calculating the positive area by the ImageJ software^{S1} at 200X magnification in 10 random micrographs taken from each main liver lobe for each animal. Portal fibrosis was calculated as percentage of pixels above the threshold value with respect to the total pixels per portal area.

Expression of $\alpha\text{v}\beta\text{6}$ integrin, Snail1, p-Smad3, and phenotypic characterization of the portal inflammatory cell infiltrate by immunohistochemistry in human and murine samples. After deparaffination, sections were hydrated in alcohol and endogenous peroxidase activity was blocked by 30min incubation in methanolic hydrogen peroxide (10%). A proper retrieval was used to unmask the antigen recognized by the primary antibody, and then the samples were rinsed in 0.05% Tween 20 in PBS (pH 7.4) and blocked with Ultra V Block (ThermoFisher, Milan, Italy) before applying the primary antibody.

Sections were incubated overnight at 4°C with the primary antibodies listed in Supplemental Table 2. Following incubation with the selected antibody, sections were rinsed with 0.05% Tween 20 in PBS for 5 min, incubated for 30 min at room temperature with the appropriated horseradish peroxidase-conjugated secondary antibody (1:100; DAKO, Denmark) and finally developed with 3,3'-diaminobenzidine. For immunofluorescent stainings, following incubation with the primary antibodies, sections were incubated with the appropriate fluorescent secondary antibody (1:500, Alexa Fluor 488 or 594, Life Technologies, USA; both in PBS + 1% bovine serum) for 30 min at room temperature. After washing in PBS and mounting using a Vectashield Kit (Vector Laboratories, Burlingame, CA, USA) with 4,6-diamidino-2-phenylindole (DAPI), the slides were examined using the Nikon Eclipse TE2000U microscope.

Quantification of K19⁺, α -SMA⁺, ELN⁺, CD45⁺, F4/80⁺/iNOS⁺ and F4/80⁺/CD206⁺ cells, and α v β 6 integrin expression. To quantify the areas positive for K19, a motorized stage system able to scan the whole liver lobes was used and bile ducts measured as the percentage of pixels above the threshold value with respect to the total pixels per area. To quantify CD45 and α v β 6 integrin, 5 random no-overlapping fields for each main liver lobe were recorded with a digital camera at 200X magnification. In these micrographs, computed morphometric analysis of CD45 immunolabeling was performed calculating the percentage of pixels above the threshold value with respect to the total pixels per slide area. The area positive for CD45 (μm^2) and the number of bile ducts positive for α v β 6 integrin were manually measured using the ImageJ software by 3 investigators blinded to the treatment code (LL, SL, MDM). To quantify α -SMA⁺, CD45⁺, ELN⁺, F4/80⁺/iNOS⁺ and F4/80⁺/CD206⁺ cells, 5 random no-overlapping fields were recorded at 200X magnification and cells coexpressing the 2 antigens were manually counted using ImageJ software by the same investigators as above.

Expression of β 6 mRNA, fibrosis-related transcripts and cyto/chemokines by quantitative real-time RT-PCR. Fifty to 100 mg of liver tissue from different ages were

homogenized in 1 mL of Trizol (Life Technologies, Milan, Italy). Template cDNA was obtained by reverse transcription of 0.5 µg total RNA using Superscript II reverse transcriptase (Life Technologies, USA) with 50 pmol random examer and 100 pmol oligo-dT primers (Promega, Mannheim, Germany). Relative transcript levels were quantified by real-time PCR on a Light Cycler (Roche, Monza, Italy). TaqMan probe and primer set were designed on published sequences using the Primer Express software (Perkin Elmer, Waltham , MA, USA), as previously reported¹⁷. Data were analyzed with the LightCycler software and normalized to the housekeeping gene β 2MG. Gene expression of a panel of chemokines (KC/CXCL1, MIP-2/CXCL2, LIX/CXCL5, IP-10/CXCL10, SDF-1/CXCL12, IL1 α , IL1 β , IL4, IL6, IL12p40, IL13, MCP-1/CCL2, MIP-1 β /CCL4, G-CSF, GM-CSF and LIF) was studied by laser capture microdissection (LCM) to evaluate the specific changes in the biliary structures of both WT and *Pkhd1^{del4/del4}* mice at 1 and 3 months (ages where biliary cysts could be captured with higher accuracy). After a rapid staining with K19 (clone TROMAIII) to specifically label cholangiocytes, frozen section (10 µm) of liver samples were microdissected under a MMI CellCut Plus laser capture microscope (MMI, USA). Total RNA from captured epithelial cells was extracted using RNeasy Plus Micro Kit (Qiagen, Mialn, Italy) according to the manufacturer's instructions. All the total RNA samples were reverse-transcribed using the High capacity cDNA reverse transcription Kit (Life Technologies, Carlsbad, CA) and the resulting cDNA was pre-amplified using the TaqMan PreAmp Master mix (2X) (Life Technologies, Milan, Italy) and the specific TaqMan probes according to the manufacturer's instructions. Real-time PCR was performed on an ABI 7500 thermocycler (Life Technologies, Milan, Italy). The relative expression of each gene was normalized to the GAPDH gene expression.

Liver non-parenchymal cell isolation and fluorescence-activated cell sorting

(FACS) analysis. Livers from *Pkhd1^{del4/del4}* and WT mice from different ages (3, 6 and 9 months) were perfused, excised, and digested in collagenase/DNase as reported². Hepatocytes

were pelleted by low-speed spins (2 x 30g, 3min), and the non-parenchymal fraction was isolated by density gradient centrifugation (4°C, 1500 X g, 20min) using 12-18% gradient Optiprep (Sigma, USA). Cells were resuspended in PBS/FBS 3% and incubated with the monoclonal antibodies (1:200, 30min, 4°C) against the following surface markers for their phenotyping: PerCP anti-mouse CD45, APC anti-mouse CD11b, FITC anti-mouse F4/80, APC anti-mouse NK-1.1, FITC anti-mouse CD19, PE anti-mouse Ly-6G (Gr-1) and PE anti-mouse CD3. Flow samples were acquired on FACSCalibur (eBioscience, San Diego, CA, USA) and analyzed using FlowJo (Tree Star, Ashland, OR, USA).

Isolation and characterization of cholangiocytes. Cholangiocytes were maintained in 25-cm² tissue culture flasks, plated on the top of rat tail collagen and cultured as polarized monolayer on an enriched medium⁵ allowing separated collection of basolateral and apical media. Biliary phenotype was confirmed by staining for K19 and acetylated α -tubulin, and monolayer formation by measuring the transepithelial resistance.

Macrophage recruitment by conditioned media from *Pkhd1*^{del4/del4} cholangiocytes. RAW264.7 cells derives from Abelson murine leukemia virus-induced tumors in a BALB/c mouse (American Type Culture Collection – ATCC, USA) *Pkhd1*^{del4/del4} cholangiocytes were cultured over semipermeable filters as monolayers and the apical and basolateral media were separately collected. RAW264.7 cells were cultured on Boyden chambers for 48h. Briefly, 5x10⁴ RAW 264.7 cells were resuspended in serum-free medium and seeded over a polyvinylpyrrolidone-free polycarbonate membrane 8 μ m-pore filters (Transwell, Costar, Milan, Italy) coated with 50 μ g/ml matrigel, placed in a Boyden microchamber 24 well plate. Recombinant protein were administered in the lower compartment and compared to controls with no cytokines. To evaluate the specificity of the recruitment of macrophages induced by CXCL1, CXCL10 and CXCL12, we used for migration experiments basolateral medium supplemented with neutralizing antibodies for CXCL1 and

CXCL10 (0.25 µg/ml and 0.20 µg/ml, respectively; both from R&D Systems, Milan, Italy) or with AMD3100 (1 µg/ml, Sigma, Milan, Italy)^{S2}. To inhibit CXCR4, RAW 264.7 cells were pretreated for 30 min with AMD31100. Cells added to the upper compartment of the chamber were incubated for 48 h at 37°C in a 5% CO₂/95% air atmosphere. To evaluate the number of fully migrated macrophages, the cells on the upper surface were removed with a cotton swab and the lower surface of the transwell filter was stained with Diff-Quick Staining Set (Medion Diagnostics, Milan, Italy) and then micrographs of 20 random fields were taken on each filter to count the number of clearly discernible nuclei.

Effects of TGFβ1 and TNFα on β6 mRNA expression on cultured cholangiocytes before and after the inhibition of the TGFβ receptor type II. After starvation for 24 h, polarized cultured cholangiocytes were treated for 24 h with recombinant murine TGFβ1 (1 ng/ml) and TNFα (1000 U/ml) (both from R&D Systems, Milan, USA). β6 mRNA expression was then evaluated in total RNA extracted with Trizol Reagent (Life Technologies, Milan, Italy) from cultured cholangiocytes, as previously described^{S3}.

Determination of cytokine secretion in *Pkhd1^{del4/del4}* cholangiocytes. For each cytokine, amounts were normalized to the total cellular protein content. To assess whether activation of β-catenin signaling could be responsible for increased cytokine production, secretion and mRNA expression of CXCL1, CXCL10 and CXCL12 was assessed in polarized cells treated with two different β-catenin inhibitors, quercetin (50 µM, Sigma, Milan, Italy) and ICG-001 (25 µM, Selleck Chemicals, Houston, TX, USA).

Assessment of macrophage production of TGFβ1 and TNFα induced by CXCL1 and CXCL10. Cultured macrophages were tested with the mouse recombinant proteins CXCL1, CXCL10 (PeproTech, London, UK) at 1 ng/ml and CXCL12 (R&D Systems, Milan, Italy) at 100 µg/ml, for 12 h.

Statistical Analysis. Results are shown as means ± SD. Statistical comparisons were

made using one-way analysis of variance (ANOVA) or the Wilcoxon–Mann–Whitney 2-sample rank sum test, where appropriate. In the latter, the p value was obtained from the exact permutation null distribution. Correlation studies were performed using Pearson's coefficient. Statistical analysis was performed using SAS software (SAS Institute Inc, Milan, Italy); p values <0.05 were considered significant.

Accepted Article

SUPPLEMENTAL FIGURES**Supplemental Figure 1. Progressive cyst development in *Pkhd1*^{del4/del4} mice. A.**

Micrographs representing liver sections taken from *Pkhd1*^{del4/del4} mice of different ages: biliary microhamartomas and cysts progressively developed in conjunction with an enlargement of the portal space (H&E staining, M=100X). **B.** Progressive enlargement in the K19⁺ cystic area (n=3/7 for each age). **p<0.01 vs WT (same age).

Supplemental Figure 2. FACS analysis and phenotyping of CD45⁺ liver non-parenchymal cell subpopulations in WT and *Pkhd1*^{del4/del4} mice. A.

In *Pkhd1*^{del4/del4} mice, the majority of the CD45⁺ cells were macrophages, based on their co-expression of CD11b and F4/80. FACS dot-plots from *Pkhd1*^{del4/del4} mice at 3 months is shown as representative analysis of n= 3. **B.** The percentage of CD45⁺/CD11b⁺/F4/80⁺ cells ranged from 57 to 68% of the total CD45⁺ liver cell population and this proportion remained substantially stable over maturation without significant changes in *Pkhd1*^{del4/del4} mice at 3, 6 and 9 months of age (n=3 for each age).

Contribution of neutrophils (CD45⁺/Ly6G⁺) and monocytes (CD45⁺/CD11b⁺/Ly6G⁻/F4/80⁻) was much lower than that of macrophages (highest relative levels for neutrophils up to 7% at month 3, for monocytes up to 13% at month 9), whereas the proportion of different lymphocyte subtypes were generally less than 10%. **C-D.** By immunoperoxidase for F4/80 (macrophage marker, **C**) and NIMP-R14 (neutrophil marker, **D**), we confirmed a progressive infiltration of macrophages in the portal space over maturation, in contrast with neutrophils, whose contribution to the inflammatory cell population was limited to small cell clumps in all ages (representative samples at 3, 6 and 9 months, n=3 for each age, M=200X). **E.** Dual immunofluorescence for CD45 (green) and F4/80 (red) confirmed that the majority of CD45⁺ cells co-expressing F4/80 (macrophages) were localized in the portal space, in close vicinity to the cyst profile (representative sample, 9 months, M=100X).

Supplemental Figure 3. Phenotypic characterization of periportal macrophage

population. A. By dual immunofluorescence with K19 (green), and MAC387 or CD68 (both red), markers for bone marrow-derived or endogenous, resident macrophages, respectively, we found that the vast majority of the periportal infiltrate was composed by recruited MAC387⁺ macrophages, whilst the proportion of CD68⁺ resident macrophages was negligible until 9 months (A, representative sample, 3 months; B, representative sample, 9 months; M=200X).

Supplemental Figure 4. CD45⁺ inflammatory cells are prevalent in the portal infiltrate of liver biopsies from CHF not yet complicated by portal hypertension. A.

Phenotypic characterization of the portal cell infiltrate in liver biopsy from a CHF patient still not evolving to portal hypertension, showed preponderance of CD45⁺ inflammatory cells over α -SMA⁺ and ELN⁺ myofibroblasts. **B.** In contrast, in a patient with more advanced disease complicated by portal hypertension, biliary cysts were surrounded by a dense accumulation of α -SMA⁺ and ELN⁺ fibroblasts of portal origin, which become prevalent on CD45⁺ cells (immunoperoxidase for CD45 and α -SMA; dual immunofluorescence for K7, green, and ELN, red, M=200X).

Supplemental Figure 5. Expression of α v β 6 integrin, Snail1 and pSmad3 in *Pkhd1*^{del4/del4} mice is present both in mice and in human CHF samples. A-D.

Expression of α v β 6 integrin on cystic bile ducts was present in both *Pkhd1*^{del4/del4} mice (**A-B**) and CHF patients (**C-D**), to a variable extent dependent upon the extension of fibrosis. Whereas α v β 6 integrin was focally expressed by biliary cysts in mice of 3 months of age (**A**) and in a patient with early disease (**C**), it decorated almost the entire perimeter of the lining epithelium in mice of 12 months of age (**B**) and in a patient with advanced disease requiring liver transplantation (**D**). α v β 6 integrin was associated with nuclear expression of Snail1 and pSMAD3, as determined in serial sections. This indicates that α v β 6-mediated TGF β 1 activation is functionally operating in cholangiocytes, in both experimental condition and human disease (Immunoperoxidase, M =

200X, insets = 400X) (n=3 for both ages for mice, n=3 for both early and advanced human CHF).

Supplemental Figure 6. CXCL1 and CXCL10 stimulate macrophage recruitment and TNF α and TGF β 1 expression. **A.** CXCL1 and CXCL10 (1ng/ml either) induced a significant stimulatory effect on transwell migration of RAW 264.7 cells of the same proportion (n=4 for each experimental group). **B-C.** RAW 264.7 cells exposed to CXCL1 and CXCL10 (1 ng/ml) showed a significant increase in the expression of TGF β 1 (**B**) and TNF α (**C**) mRNA levels, while CXCL12 (100 μ g/ml) did not induce any significant change in macrophage expression of these cytokines (n=4 for each experimental group). *p<0.05 vs Ctrl.

Supplemental Figure 7. TGF β 1 stimulate gene expression of Snail1 and procollagen-I in *Pkhd1^{del4/del4}* cholangiocytes. **A-B.** With respect to WT, *Pkhd1^{del4/del4}* cholangiocytes showed increased basal mRNA levels of COL1(A1) (**A**) as well as of Snail1 (**B**), which were both strongly stimulated by TGF β 1 at low doses (1 ng/ml) (n=4). Interestingly, TGF β 1-stimulated COL1(A1) production was a specific property of *Pkhd1^{del4/del4}* cholangiocytes, not found in WT cells. **C.** Consistent with this *in vitro* finding, increased mRNA levels of COL1(A1) were detected *in vivo* in biliary cysts of *Pkhd1^{del4/del4}* mice selectively captured by LCM at 1 and 3 months (n=3 for WT, n=4 for *Pkhd1^{del4/del4}* for both ages). **D.** Collagen-I deposition along the biliary cyst profile was observed in histological tissue sections (representative sample of n=3, 3 months, dual immunofluorescence of K19 – green, with Collagen I - red, M=200X). *p<0.05 vs WT, **p<0.01 vs WT, ^p<0.05 vs ctrl, ^^p<0.01 vs Ctrl, °p<0.05 vs WT (same age), °°p<0.01 vs WT (same age).

Supplemental Figure 8. Effects of clodronate treatment on biliary cyst enlargement in *Pkhd1^{del4/del4}* mice. **A-B.** Micrographs representing liver sections taken from control animals (vehicle) (A) and from *Pkhd1^{del4/del4}* mice treated with clodronate, from the 3rd through the

6th month (B). In clodronate treated mice, an evident improvement of histological features related to portal inflammation and fibrosis could be noticed (H&E representative sample, M=200X). C-D. Moreover, by computer-assisted morphometry, cystic area resulted significantly decreased in clodronate-treated mice with respect to controls (K19 representative sample, M=100X). E. A reduction of the cystic area greater than 50% was observed in clodronate-treated mice (**p<0.01 vs vehicle).

Supplemental Figure 9. Effects of clodronate treatment in *Pkhd1*^{del4/del4} mice on peribiliary fibrosis, $\alpha\beta6$ integrin expression on biliary cysts, macrophage infiltration and myofibroblast activation in the portal tract. A-D. Representative images of the decreasing effects of a 3-month treatment of clodronate in *Pkhd1*^{del4/del4} mice with respect to vehicle on portal infiltration of macrophages (red immunofluorescence for F4/80, M=400X, A) and myofibroblasts (dual immunofluorescence for α -SMA - red, and CK19 - green, M=200X, B), $\alpha\beta6$ integrin expression on biliary structures (immunoperoxidase, M=200X, C), and peribiliary fibrosis (Sirius Red staining, M=200X, D) (n=3 vehicle, n= 4 clodronate treated).

SUPPLEMENTAL REFERENCES

- S1. Hadi AM, Mouchaers KT, Schaliij I, Grunberg K, Meijer GA, Vonk-Noordegraaf A, et al. Rapid quantification of myocardial fibrosis: a new macro-based automated analysis. *Cell Oncol.* 2011;34, 343-354.
- S2. Gentilini A, Rombouts K, Galastri S, Caligiuri A, Mingarelli E, Mello T, et al. Role of the stromal-derived factor-1 (SDF-1)-CXCR4 axis in the interaction between hepatic stellate cells and cholangiocarcinoma. *J Hepatol.* 2012;57, 813-820.
- S3. Spirli C, Fabris L, Duner E, Fiorotto R, Ballardini G, Roskams T, et al. Cytokine-stimulated nitric oxide production inhibits adenylyl cyclase and cAMP-dependent secretion in cholangiocytes. *Gastroenterology.* 2003;124, 737-753.

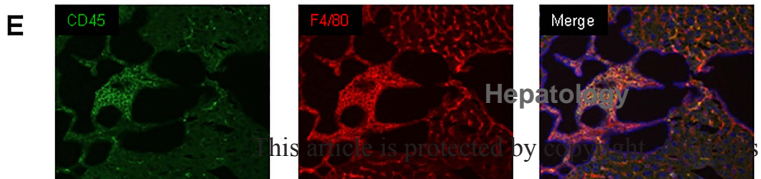
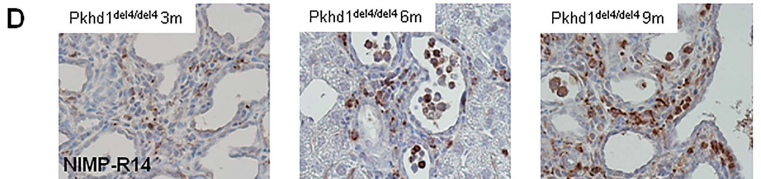
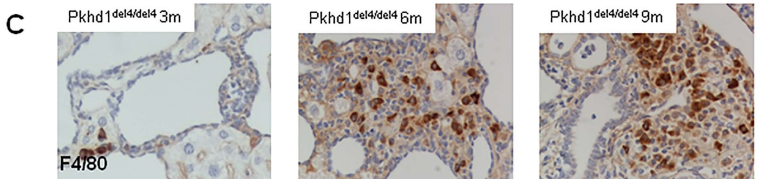
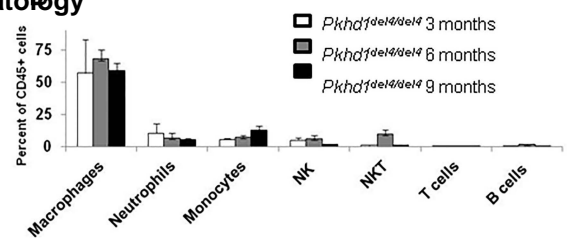
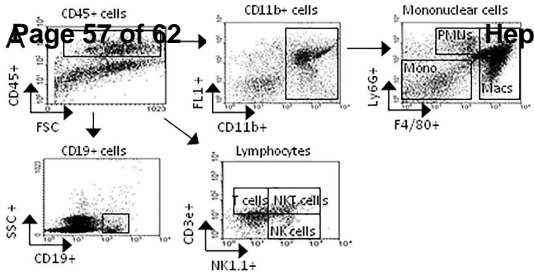
Supplemental Table 1. Panel of 32 cyto/chemokines evaluated by Luminex assay/ELISA in basolateral conditioned medium of polarized cholangiocyte monolayer (pg/mg prot).

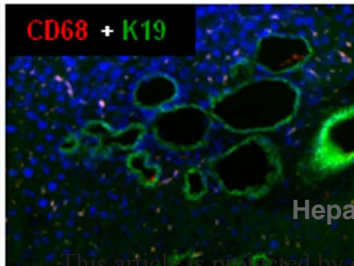
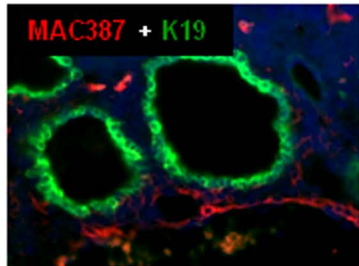
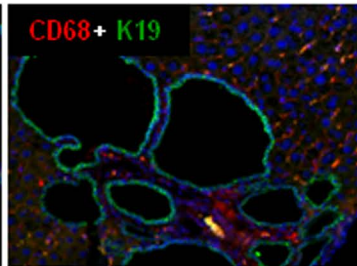
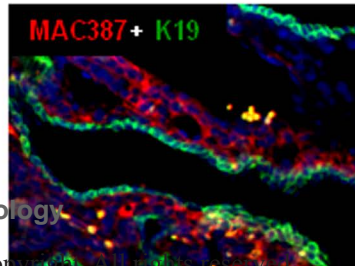
	WT	<i>Pkhd1</i>^{del4/del4}		WT	<i>Pkhd1</i>^{del4/del4}	
G-CSF	89,50±96,87	281,92±308,4 1		IL-17	0,31±0,28	0,35±0,30
GM-CSF	10,51±9,22	8,94±7,75		KC/CXCL1*	15,08±2,91	31,09±1,42
IL-1α	7,41±6,20	14,53±19,06		MIP-2/CXCL2	ND	27,43±23,76
IL-2	0,28±0,28	0,22±0,19		LIX/CXCL5	12,34±11,03	103,81±89,90
IL-3	0,86±0,76	0,74±0,64		IP-10/CXCL10*	3,39±0,26	7,44±0,42
IL-5	0,24±0,40	0,26±0,23		SDF-1/CXCL12*	0,45±0,12	0,83±0,16
IL-6	1,33±1,17	1,93±1,68		MCP-1/CCL2	96,98±100,82	194,98±282,29
IL-7	0,6±0,53	0,58±0,50		MIP-1β/CCL4	6,41±5,82	0,99±0,86
IL-10	0,11±0,11	0,37±0,32		RANTES/CCL5	1,05±0,92	1,13±0,98
IL-12 (p40)	5,95±6,09	4,37±3,79		LIF	10,30±10,88	28,48±30,94
IL-13	9,93±9,34	11,66±14,07		TNF-α	0,95±0,83	0,91±0,79
IL-15	1,04±1,81	1,48±1,29				

Eotaxin, IFN- γ , IL-1 β , IL-4, IL-9, IL-12 (p70), M-CSF, MIG/CXCL9 and MIP-1 α /CCL3 were not detectable (ND) both and in WT and *Pkhd1*^{del4/del4} cholangiocytes; *p<0.05 vs WT

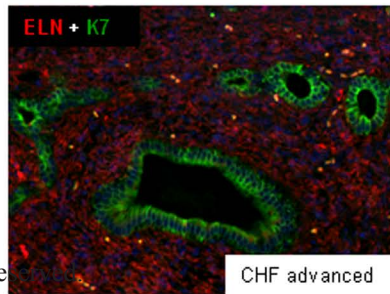
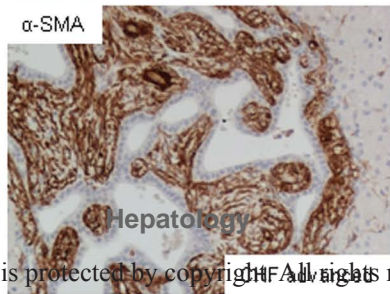
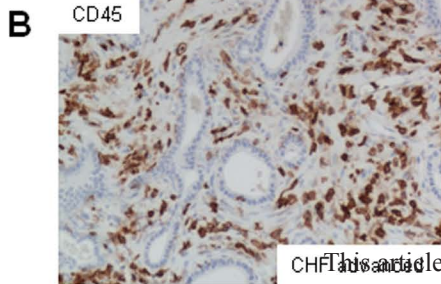
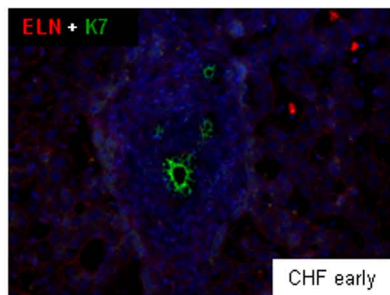
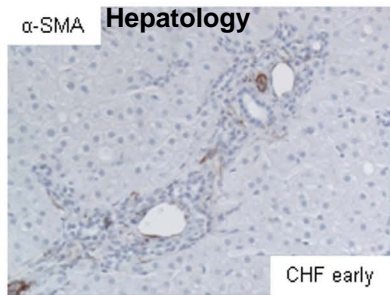
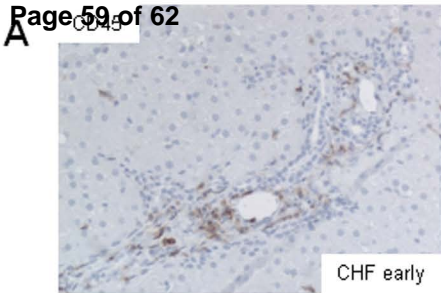
Supplemental Table 2. List of primary antibodies used for immunohistochemistry.

	Clone	Supplier	Dilution
α -SMA	1A4	DAKO	1:100
Anti-Macrophage (calprotectin or L1)	MAC387	Abcam	1:100
α v β 6 integrin (mouse)	ch2A1	Stromedix/Biogen	1:500
α v β 6 integrin (human)	6.2A1	Stromedix/Biogen	1:500
CD206	polyclonal	Bioss Inc.	1:100
CD45 (mouse)	30-F11	BD Pharmingen	1:20
CD45 (human)	2B11 + PD7/26	DAKO	1:300
CD68	ED1	Abcam	1:500
Cytokeratin-19 (K19)	Troma III	Hybridoma Bank University of Iowa	1:200
Collagen-I	polyclonal	Sigma	1:100
Elastin	10B8	LifeSpan Bioscience	1:100
F4/80	BM8	eBioscience	1:100
iNOS	polyclonal	Abcam	1:200
NIMP-R14	polyclonal	Santa Cruz Biotechnology	1:100
p-Smad3	polyclonal	Rockland Immunochemicals	1:200
Snail1	polyclonal	Abcam	1:100



A*Pkhd1^{del4/del4}* 3 m**Hepatology****B***Pkhd1^{del4/del4}* 9 m**Page 58 of 62****Hepatology**

This article is protected by copyright. All rights reserved.



$\alpha v\beta 6$

Snail1

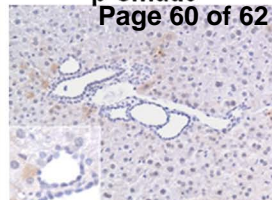
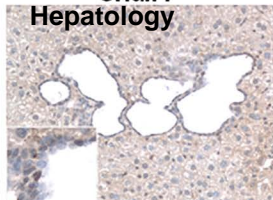
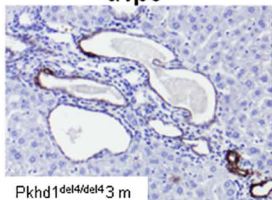
p-Smad3

Hepatology

Page 60 of 62

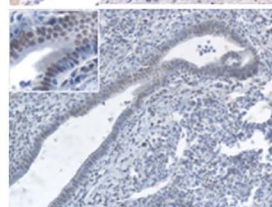
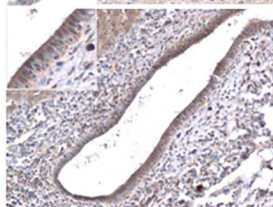
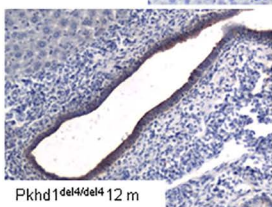
A

Mouse



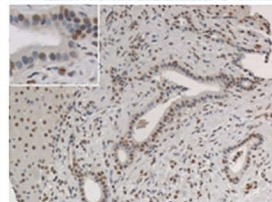
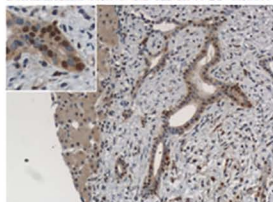
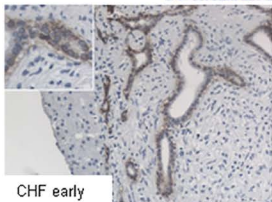
B

Mouse



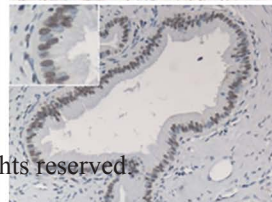
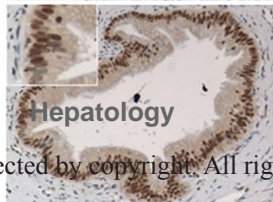
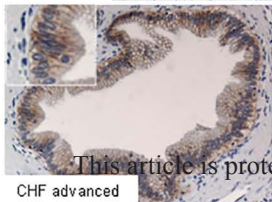
C

Human



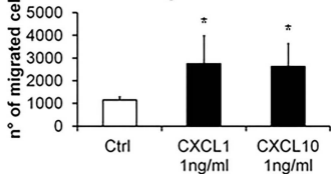
D

Human



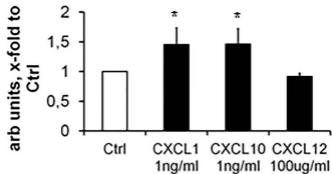
This article is protected by copyright. All rights reserved.

Cell migration



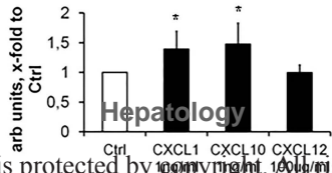
B

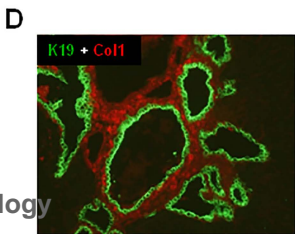
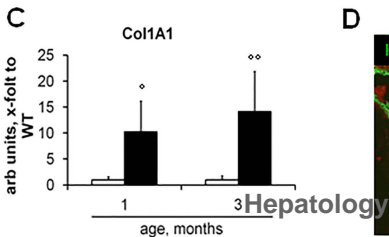
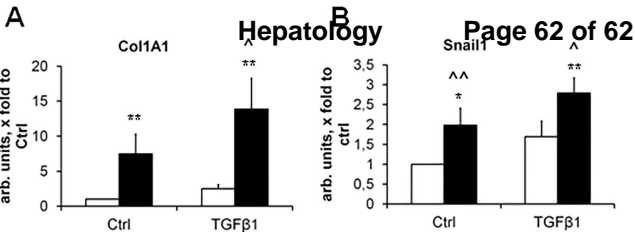
TGFβ1

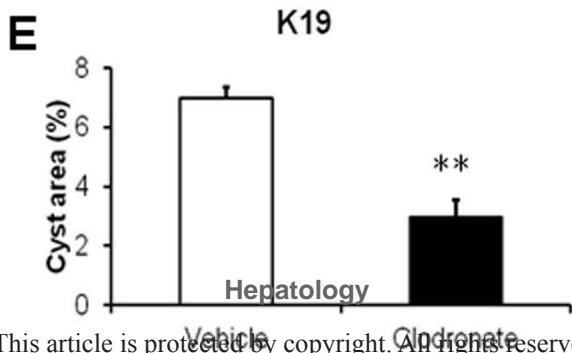
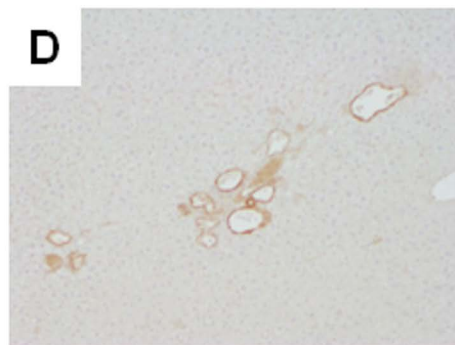
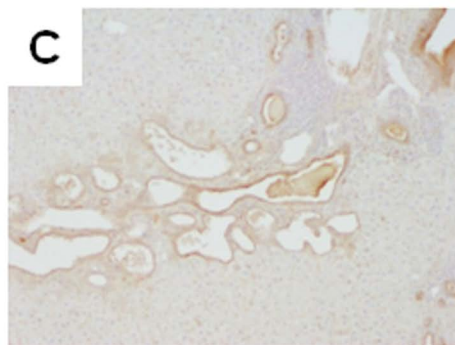
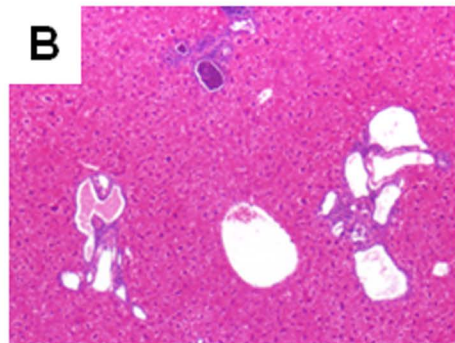
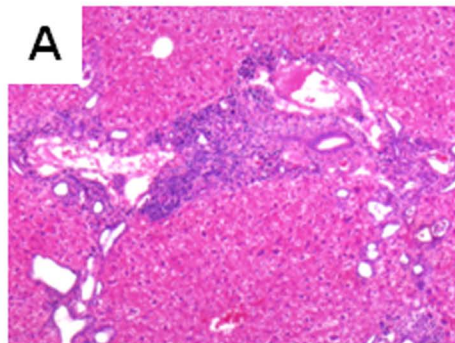


C

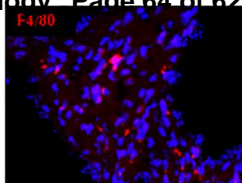
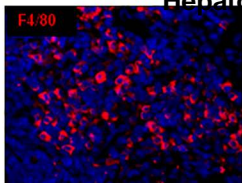
TNFα



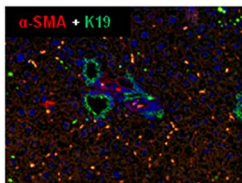
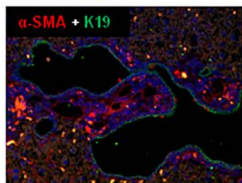




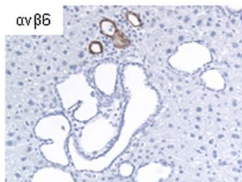
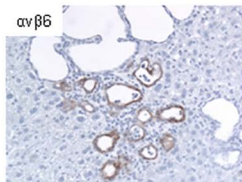
A



B



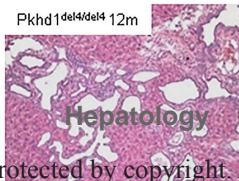
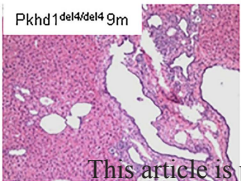
C



D



Hepatology



B

